



Improving U.S. National Water Model Streamflow with Long Short-Term Memory Networks

Journal:	<i>Journal of the American Water Resources Association</i>
Manuscript ID	JAWRA-20-0099-P.R1
Manuscript Type:	Technical Paper
Date Submitted by the Author:	n/a
Complete List of Authors:	Frame, Jonathan; University of Alabama, Geological Sciences Nearing, Grey; Google Research Kratzert, Frederik; Johannes Kepler University, LIT AI Lab & Institute for Machine Learning Raney, Austin; University of Alabama, Geography Rahman, Mashrekur; University of Alabama, Geological Sciences Salas, Fernando R.; NOAA, NWS Office of Water Prediction
Category Headings:	HYDROLOGY, MODELING
Key Terms:	streamflow < HYDROLOGY, National Water Model, long short-term memory, post-processing, machine learning

Revised manuscript submitted to the Journal of The American Water Resources Association (JAWRA) March 2021

1
2
3 30 **(KEYWORDS:** National Water Model; theory-guided machine learning; long short-term
4
5 31 memory; streamflow; model diagnostics.)
6
7
8
9
10
11
12
13
14
15
16
17
18
19
20
21
22
23
24
25
26
27
28
29
30
31
32
33
34
35
36
37
38
39
40
41
42
43
44
45
46
47
48
49
50
51
52
53
54
55
56
57
58
59
60

For Peer Review

INTRODUCTION

The U.S. National Water Model (NWM), based on WRF-Hydro (Cosgrove *et al.*, 2015), is an emerging large-scale hydrology simulator. Some specific details of the NWM advancements in large scale hydrology are described by Elmer (2019, page 11), including increased resolution and number of stream reaches (2.7 million) for a model covering the continental United States (CONUS). A purported strength of WRF-Hydro is simulating hydrologic dynamics, and specifically timing of hydrological response (Salas *et al.*, 2018). The predictive performance of the NWM (ability to match streamflow observations) has been shown to vary widely. Hansen *et al.* (2019) evaluated the performance of the NWM in the Colorado River Basin in terms of drought and low flows; they found better performance in the Upper Colorado River Basin than in the Lower Colorado River Basin, and attributed this discrepancy to the NWM's ability to simulate snowpack. WRF-Hydro has generally poor performance in the Southwest and Northern Plains (Salas *et al.*, 2018). Salas *et al.*, 2018 hypothesized that error in WRF-hydro might come from lakes, reservoirs, floodplain dynamics and soil parameter calibration.

The NWM version 2.0 was calibrated at 1,457 basins within the CONUS domain. As a point of comparison, the United States Geological Survey (USGS) records daily streamflow at 28,529 basins (<https://nwis.waterdata.usgs.gov/nwis>, accessed June 2020). Calibrating the model at each stream gauge within the NWM domain is a large computational expense, and while regionalization strategies can be used to improve forecast accuracy without having to calibrate each individual basin, accuracy typically suffers compared to direct calibration. Due to these reasons and others, making accurate hydrological predictions over large scales is a challenging

1
2
3 54 problem, however there are promising results in the machine learning and data science
4
5 55 communities that may be directly applicable to improving the NWM.
6
7

8 56 Machine learning (ML) is a powerful tool for hydrological modeling, and there has been
9
10 57 a call to merge ML with traditional hydrological modeling (Reichstein *et al.*, 2019; Nearing et
11
12 58 al., 2020). One example of an ML approach that has been effective for hydrological prediction is
13
14 59 the “long short-term memory” network (LSTM) (Hochreiter, 1991; Hochreiter and Schmidhuber,
15
16 60 1997). The LSTM is a time series deep learning method that is particularly well suited to model
17
18 61 hydrologic processes because it mimics in certain ways the Markovian input-state-output
19
20 62 structure of a dynamical system (Kratzert *et al.*, 2018). LSTMs have been effective at simulating
21
22 63 predictions of surface runoff at the daily time scale (Kratzert *et al.*, 2019a), including in
23
24 64 ungauged catchments where traditional methods of calibration do not work (Kratzert *et al.*,
25
26 65 2019b), and also at sub-daily (hourly) timescales (Gauch et al., 2020). One potential problem
27
28 66 with ML, however, is that it lacks a physical basis. While there are emerging efforts in hydrology
29
30 67 to merge physical understanding with machine learning (Karpatne *et al.*, 2017a; Daw *et al.*,
31
32 68 2020; Pelissier *et al.*, 2019; Chadalawada *et al.*, 2020; Tartakovsky *et al.*, 2020, Read et al.,
33
34 69 2019; Nearing et al., 2020; Hoedt et al., 2021), the field of *theory-guided machine learning*
35
36 70 (Karpatne *et al.*, 2017b) is still relatively immature in hydrology.
37
38
39
40
41
42
43

44 71 The NWM informs forecasts of many hydrologic conditions, including river ice,
45
46 72 snowpack, soil moisture and inundation, which are used for management applications such as
47
48 73 transportation, recreation, agriculture and fisheries (NOAA 2019). When ML is to be used in the
49
50 74 NWM it should not disrupt the delivery of these hydrologic forecasts, therefore an ML prediction
51
52 75 for streamflow that does not also include predictions of the other hydrologic states and variables
53
54 76 must be run in parallel with the existing process-based hydrologic model. A natural question
55
56
57
58
59
60

1
2
3 77 arises: does the existing NWM formulation benefit the already highly accurate LSTM predictions
4
5 78 of streamflow?
6
7

8
9 79 Hydrologic post-processing can remove systematic errors in the model prediction, and
10
11 80 has been shown to improve forecast accuracy of both calibrated and uncalibrated basins,
12
13 81 particularly in wet basins (Ye *et al.*, 2014). The general methodology of post-processing involves
14
15 82 taking the output of a process-based model and feeding it into a data-driven model. In this paper
16
17 83 we applied a LSTM-based post-processor for the NWM to improve basin-scale streamflow
18
19 84 predictions. This is a straightforward theory-guided machine learning approach. We tested a
20
21 85 post-processor that uses dynamic information only from the NWM outputs and compared the
22
23 86 results against the NWM itself. We also tested a post-processor that included both the NWM
24
25 87 outputs and NLDAS atmospheric forcings as inputs and compared against a ‘baseline’ LSTM
26
27 88 model trained only with atmospheric forcings (no NWM outputs).
28
29
30
31

32 89 We applied the LSTM post-processors to 531 basins across the CONUS. The basins
33
34 90 chosen for this large-scale analysis are mostly headwater catchments without engineered control
35
36 91 structures, such as dams, canals, and levees. This was a deliberate choice made for the purpose of
37
38 92 simulating a close-to-natural rainfall-runoff response. Our goal was to use the post-processor to
39
40 93 learn systematic corrections to simulated basin-scale rainfall-runoff processes that can improve
41
42 94 forecasts of streamflow, rather than the hydraulic engineering implications resulting from
43
44 95 simulated controlled flow, *e.g.*, a reservoir release. Kim *et al.* (2020) showed the limitation of the
45
46 96 NWM to predict streamflow in a highly engineered watershed and the need for representing
47
48 97 controlled releases. Thus, we are using some of the simplest, and top performing, applications of
49
50 98 the NWM for these experiments.
51
52
53
54
55

56 99 **METHODS**

1
2
3 100 *Data & Models*
4
5

6 101 **CAMELS Catchments.** This study used the Catchment Attributes and Meteorological
7
8 102 dataset for Large Sample Studies (CAMELS) (CAMELS; Newman *et al.*, 2015; Addor *et al.*,
9
10 103 2017). These data were curated by the US National Center for Atmospheric Research (NCAR;
11
12 104 <https://ral.ucar.edu/solutions/products/camels>, accessed March 2020), and we used the 531 (out
13
14 105 of 671) basins that were chosen by Newman *et al.* (2015) for model benchmarking. Newman et
15
16 106 al (2015) excluded basins with large discrepancies in different methods for measuring basin area
17
18 107 and also basins larger than 2,000 km². CAMELS data include corresponding daily streamflow
19
20 108 records from USGS gauges, and meteorological forcing data (precipitation, max/min
21
22 109 temperature, vapor pressure and total solar radiation) come from North American Land Data
23
24 110 Assimilation System (NLDAS; Xia *et al.*, 2012).
25
26
27
28
29

30 111 **National Water Model.** We used the National Water Model version 2.0 reanalysis,
31
32 112 which contains output from a 25-year (January 1993 through December 2019) retrospective
33
34 113 simulation (<https://docs.opendata.aws/nwm-archive/readme.html>, accessed June 2020). The
35
36 114 NWM retrospective ingests rainfall and other meteorological forcings from atmospheric
37
38 115 reanalyses (<https://water.noaa.gov/about/nwm>, accessed June 2020.). NWM reanalysis output
39
40 116 includes channel outputs (point fluxes: CHRT) and land surface (gridded states and fluxes:
41
42 117 LDAS & RT) outputs. The specific features that we used from the NWM reanalysis are shown in
43
44 118 Table 1. To be compatible with the LSTM model, which uses a one-day timestep and was trained
45
46 119 using all basins simultaneously, we took the mean values of these model outputs across UTC
47
48 120 calendar days (12AM - 11PM) to produce daily records from the hourly NWM when used as
49
50 121 input to the LSTM, but for NWM streamflow diagnostics we used the local calendar day (based
51
52 122 on U.S. time zone) to be compatible with the USGS gauge records. Channel routing point data
53
54
55
56
57
58
59
60

1
2
3 123 (CHRT) were collected at each individual NWM stream reach that corresponds to the stream
4
5 124 gauge associated with each CAMELS catchment. Gridded land surface data (LDAS) was
6
7 125 collected from each 1 km² Noah-MP cell contained within the boundaries of each CAMELS
8
9 126 catchment, and these were averaged to produce a single representative (lumped) value for each
10
11 127 catchment. Gridded routing data (RT) were collected from each 250 m² cell, and we included the
12
13 128 mean and maximum value within the catchment boundary. We did not include lake input and
14
15 129 output fluxes because these would be inconsistent across basins (some basins have zero and
16
17 130 some basins have multiple lakes). Note that the units of the NWM outputs are not required for
18
19 131 the LSTM post-processor.
20
21
22
23

24 132 TABLE 1. National Water Model Output Data

Feature name	Feature	NWM model component	Resolution
ACCET	Accumulated evapotranspiration	LDAS	1Km
FIRA	Total net long-wave (LW) radiation to atmosphere	LDAS	1Km
FSA	Total absorbed short-wave (SW) radiation	LDAS	1Km
FSNO	Snow cover fraction on the ground	LDAS	1Km
HFX	Total sensible heat to the atmosphere	LDAS	1Km
LH	Latent heat to the atmosphere	LDAS	1Km
SNEQV	Snow water equivalent	LDAS	1Km
SNOWH	Snow depth	LDAS	1Km
SOIL M (4 layers)	Volumetric soil moisture	LDAS	1Km
SOIL W (4 layers)	Liquid volumetric soil moisture	LDAS	1Km
TRAD	Surface radiative temperature	LDAS	1Km
UGDRNOFF	Accumulated underground runoff	LDAS	1Km
streamflow	River Flow	CHRT	point
q_lateral	Runoff into channel reach	CHRT	point
velocity	River Velocity	CHRT	point
qSfcLatRunoff	Runoff from terrain routing	CHRT	point
qBucket	Flux from groundwater bucket	CHRT	point
qBtmVertRunoff	Runoff from bottom of soil to groundwater bucket	CHRT	point
Sfheadsbrt (mean and max)	Ponded water depth	RTOUT	250Km
Zwattablrt (mean and max)	Water table depth	RTOUT	250Km

51 133
52
53
54
55
56
57
58
59
60

1
2
3 134 **Long short-term memory network.** The LSTM is a recurrent neural network that is able
4
5 135 to maintain a memory of the system state and dynamics through a period of time (in this case 365
6
7 136 days). This recurrent state space is the main advantage for hydrological applications over other
8
9
10 137 types of neural networks. Our LSTM network was developed from Kratzert et al. (2019) using a
11
12 138 codebase that is now referred to as NeuralHydrology (<https://neuralhydrology.github.io/> accessed
13
14 139 March 2021). This research grade codebase was developed in the Python programming language
15
16
17 140 and is based primarily on the Pytorch machine learning library.
18
19

20 141 The LSTM used two types of inputs: daily meteorological forcings and static catchment
21
22 142 attributes. Again, note that the units of the forcing data are irrelevant when used as inputs for the
23
24 143 LSTM, which does not include a mass or energy balance. We normalized all inputs to the LSTM,
25
26 144 including static and dynamic inputs by subtracting the mean and dividing by the standard
27
28 145 deviation of the training data. We used eighteen catchment attributes from the CAMELS dataset
29
30 146 related to climate, vegetation, topography, geology, and soils. These are described in more detail
31
32 147 by Addor *et al.* (2017) and listed here in Table 2. Catchment attributes are static for each basin
33
34 148 (do not change in time). For the post-processing runs we added the states, fluxes, and streamflow
35
36 149 predictions from version 2.0 of the NWM.
37
38
39
40

41 150 TABLE 2. LSTM Inputs

Meteorological Forcing Data (used in models denoted with an “A”)	
Maximum Air Temp (TMax)	2-meter daily maximum air temperature
Minimum Air Temp (TMin)	2-meter daily minimum air temperature
Precipitation (PRCP)	Average daily precipitation
Radiation (SRAD)	Surface-incident solar radiation
Vapor Pressure (Vp)	Near-surface daily average
Static Catchment Attributes (used in each of the LSTM models)	
Precipitation Mean	Mean daily precipitation
PET Mean	Mean daily potential evapotranspiration
Aridity Index	Ratio of Mean PET to Mean Precipitation
	Estimated by representing annual precipitation and temperature as sin waves
Precipitation Seasonality	Positive (negative) values indicate precipitation peaks during the summer (winter).

1		Values of approx. 0 indicate uniform precipitation throughout the year.
2		
3		
4	Snow Fraction	Fraction of precipitation falling on days with temp [C].
5		Frequency of days with $\leq 5x$ mean daily precipitation. Average duration of high
6		precipitation events (number of consecutive days with $\leq 5x$ mean daily
7	High Precipitation Frequency	precipitation).
8	Low Precipitation Frequency	Frequency of dry days (< 1 mm/day).
9		Average duration of dry periods (number of consecutive days with precipitation < 1
10	Low Precipitation Duration	mm/day).
11	Elevation	Catchment mean elevation.
12	Slope	Catchment mean slope.
13	Area	Catchment area.
14	Forest Fraction	Fraction of catchment covered by forest.
15	LAI Max	Maximum monthly mean of leaf area index.
16	LAI Difference	Difference between the max. and min. mean of the leaf area index.
17	GVF Max	Maximum monthly mean of green vegetation fraction.
18		Difference between the maximum and minimum monthly mean of the green
19	GVF Difference	vegetation fraction.
20	Soil Depth (Pelletier)	Depth to bedrock (maximum 50m).
21	Soil Depth (STATSGO)	Soil depth (maximum 1.5m).
22	Soil Porosity	Volumetric porosity.
23	Soil Conductivity	Saturated hydraulic conductivity.
24	Max Water Content	Maximum water content of the soil.
25	Sand Fraction	Fraction of sand in the soil.
26	Silt Fraction	Fraction of silt in the soil.
27	Clay Fraction	Fraction of clay in the soil.
28	Carbonate Rocks Fraction	Fraction of the catchment area characterized as “carbonate sedimentary rocks”.
29	Geological Permeability	Surface permeability (log10).
30		
31		
32		
33	151	
34		
35		
36	152	We trained the LSTM models to make predictions at all 531 CAMELS catchments used
37		
38	153	in the analysis. We split the data temporally into a training period and testing period, and we
39		
40	154	present no results from the training period as these results are unrepresentative of the out-of-
41		
42	155	sample predictions. We trained the LSTMs on water years 2004 through 2014 and tested on
43		
44		
45	156	water years 1994 through 2002. No spatial splits were included in the training procedure. The
46		
47	157	LSTMs used a 365-day LSTM look-back period, so a full year gap was left between training and
48		
49	158	testing to prevent bleedover (<i>i.e.</i> , information exchange) between the two periods. We trained
50		
51	159	separate LSTMs with ten unique random seeds for initializing weights and biases, and calculated
52		
53		
54	160	benchmarking statistics using the ensemble mean hydrograph. The LSTMs make predictions
55		
56		
57		
58		
59		
60		

161 representing runoff in units [mm], reflecting an area normalized volume of water that moves
 162 through a stream at each model timestep. USGS gauge records (and the NWM predictions) are in
 163 streamflow units [L^3/T]. We used the geospatial fabric estimate of the catchment area provided
 164 in the CAMELS dataset to convert all streamflow to units [L] for our diagnostic comparison. We
 165 trained the LSTMs with the protocol and features described in Appendix B of Kratzert et al.
 166 (2019b): this includes 30 epochs, a hyperbolic tangent activation function, a hidden layer size of
 167 256 cell states, a look-back of 365 days, variable learning rates set at epoch 0 to 0.001, epoch 11
 168 to 0.005 and epoch 21 to 0.0001, dropout rate of 0.4 and an input sequence length: 270.

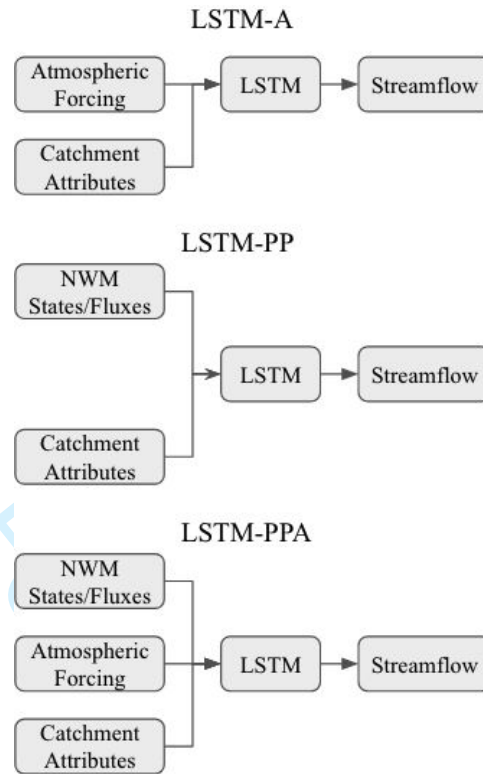
169 *Experimental Design*

170 We tested the results from LSTM post-processing against the NWM and also against a
 171 baseline LSTM with no inputs from the NWM (referred to as LSTM_A, in which the A stands
 172 for atmospheric forcing). Table 3 will guide the reader through the setup of each model.

173 TABLE 3. Models

Model label	Number of dynamic LSTM inputs	Model description
NWM	N/A	National Water Model mean daily streamflow predictions
LSTM_PP	28	LSTM trained with NWM output for post processing
LSTM_PPA	32	LSTM trained with NWM output and atmospheric forcings for post-processing
LSTM_A	5	LSTM trained with atmospheric forcing conditions.

174
 175 Simple schematics of the LSTMs used in this study are shown in Figure 1. The LSTM
 176 post-processors (LSTM_PP & LSTM_PPA) used NWM outputs as LSTM inputs, and the results
 177 were LSTM-based streamflow predictions influenced by the process-based NWM. This is a
 178 straightforward method of theory-guided machine learning.



179

180 FIGURE 1. Flow chart showing the baseline LSTM (LSTM_A) and the LSTM post-processors with NWM data as
 181 inputs (LSTM_PP & LSTM_PPA). LSTM_PP is the post-processor which used only NWM outputs as input to an
 182 LSTM, and LSTM_PPA used both the NWM outputs and atmospheric forcings.

183 As a quality check, we compared the results from each LSTM ensemble member, and
 184 found a relative standard error of the mean streamflow about 1%, and relative standard error of
 185 the Nash-Sutcliffe Efficiency (NSE) value of about 0.01%. This means that all LSTM solutions
 186 are similar between random initialization seeds. Gauch *et al.* (2019) attributed a 0.01 discrepancy
 187 in NSE values of the LSTM predictions to non-determinism of the loss function minimization. In
 188 our experiments discrepancies in the loss function occur between different random seed
 189 initializations, but running the training procedure twice with the same random seed gives an
 190 identical solution, satisfying the definition of determinism.

1
2
3 191 **Performance metrics.** We calculated several metrics to evaluate predictive performance,
4
5 192 including the NSE and Kling-Gupta Efficiency (KGE) values (Gupta et. al, 2009). The variance,
6
7 193 bias and Pearson correlation metrics were calculated separately as components of the NSE
8
9 194 (Gupta *et al.*, 2009); these tell us about relative variability, mass conservation and linear
10
11 195 correlation between the modeled/observed streamflow values, respectively. Observed streamflow
12
13 196 values are from the USGS streamflow gauges associated with each of the CAMELS basins. The
14
15 197 metrics were calculated in two ways: 1) at each basin and then averaged together, and 2) using
16
17 198 all of the flows from all basins combined.

18
19
20
21
22 199 Our graphical results focus on three performance metrics: (i) NSE measures the overall
23
24 200 predictive performance as a correlation coefficient for the 1:1 linear fit between simulations and
25
26 201 observations, (ii) Peak timing error measures the absolute value of differences (in units days)
27
28 202 between simulated and observed peak flows for a given event, and (iii) total (absolute) bias
29
30 203 measures the overall bias of the simulated hydrograph relative to observations and represents
31
32 204 how well the model matches the total volume of partitioned rainfall that passes through the
33
34 205 stream gauge at each basin.

35
36
37
38
39 206 We also calculated performance metrics on different flow regimes. Rising limbs and
40
41 207 falling limbs were characterized by a one-day derivative, where positive derivatives were
42
43 208 categorized as rising limb, and negative derivatives as falling limb. High flows were
44
45 209 characterized as all flow above the 80th percentile in a given basin, and low flows as below the
46
47 210 20th percentile in a given basin.

48
49
50
51 211 We tested the performance of the LSTM post-processors in different regions. We split the
52
53 212 basins by USGS designated “water resource regions” (<https://water.usgs.gov/GIS/regions.html>),
54
55
56
57
58
59
60

213 accessed July 2020). To analyze the regions individually we averaged the NSE, bias and timing
 214 error of the CAMELS basins within each region.

215 We set an alpha value for statistical significance to $\alpha = 0.05$. To control for multiple
 216 comparisons we adjusted the alpha values using family-wise error rate equal to $1-(1-\alpha)^m$, with m
 217 being the number of significance tests (86 in total), which brought our effective alpha value
 218 down to 0.049. We tested for statistical significance with a Wilcoxon signed-rank test against the
 219 null hypothesis that our test models (LSTM post-processors) performance across basins came
 220 from the same distribution as our base models (NWM & LSTM_A).

221 **Simulated hydrograph representation of hydrologic signatures.** Hydrologic
 222 signatures help us understand how well a model represents important aspects of real-world
 223 streamflow, and where improvement should be made to the model's conceptualization (Gupta *et*
 224 *al.*, 2008). We analyzed the hydrologic signatures described by Addor *et al.* (2018), and these are
 225 listed below in Table 4. We calculated the true signatures with USGS streamflow observations,
 226 and calculated model representations with predicted values of daily streamflow. The comparison
 227 between true values and predicted values was made with a correlation coefficient (r^2) across
 228 basins (one value of the observed and predicted hydrologic signatures were calculated per basin),
 229 higher values indicate better representation of hydrologic signature across basins by the model.
 230 We used the Steiger method to test for statistically significant improvement (or detriment)
 231 between the base models and the LSTM post-processor (Steiger and Browne, 1984).

232 TABLE 4. Hydrologic signatures (adapted from Addor *et al.* 2018)

Signature description	Signature name
Average duration of low-flow events	low_q_dur
Frequency of days with zero flow	zero_q_freq
Average duration of high-flow events	high_q_dur
Streamflow precipitation elasticity	stream_elas

Revised manuscript submitted to the Journal of The American Water Resources Association (JAWRA) March 2021

Frequency of high-flow days	high_q_freq
Slope of the flow duration curve	slope_fdc
Frequency of low-flow days	low_q_freq
Baseflow index	baseflow_index
Runoff ratio	runoff_ratio
Mean half-flow date	hfd_mean
5 percent flow quantile	q5
95 percent flow quantile	q95
Mean daily discharge	q_mean

233

234 **Identifying basins best suited for post-processing with multi-linear regression.** The

235 LSTM post-processors did not improve performance at every basin. It therefore would be

236 valuable to know if a LSTM post-processor will work in any particular basin before

237 implementation. We trained a multi-linear regression, using the Scikit-learn library in Python, to

238 predict the performance changes between the NWM and the LSTM post-processors (LSTM_PP

239 & LSTM_PPA) at each individual basin. The inputs to the regression analysis were the

240 performance score of the NWM streamflow predictions, hydrologic signatures and catchment

241 characteristics. These regressors are useful to help interpret what basins might benefit most from

242 an LSTM post-processor. We trained and tested multi-linear regression models using k-fold

243 cross-validation with 20 splits ($k=20$) over the 531 basins. We report the correlation (r^2) of out-

244 of-sample regression predictions of post-processing improvements vs. actual post-processing

245 improvements.

246 **Interpretation of LSTM with integrated gradients.** We aim to explain the relationship

247 between a model's predictions in terms of its features. This will help us understand feature

248 importance, identifying data issues, and inform NWM process diagnostics from the post-

249 processors. We calculated integrated gradients (Sundararajan *et al.*, 2017) to attribute the LSTM

250 inputs (both atmospheric forcings and NWM outputs) to the total prediction of streamflow.

1
2
3 251 Integrate gradients are a type of sensitivity analysis that are relatively insensitive to low gradients
4
5 252 (*e.g.*, at the extremes of neural network activation functions). We calculated integrated gradients
6
7 253 separately for each input, at each timestep, for each lookback timestep, in each basin. This means
8
9
10 254 that for 9 years of test data with a 365-day lookback there were about 1.2 million integrated
11
12 255 gradients per input, per basin. The unit of the integrated gradient is technically normalized
13
14 256 streamflow, but we were mostly interested in the relative values of integrated gradients of each
15
16 257 individual LSTM input.

20 258 **Interpretation of LSTM with correlations between performance and NWM inputs.**

21
22 259 We made a direct connection between LSTM post-processor improvements with the NWM
23
24 260 outputs using correlation. We calculated Pearson R values between the basin average value of
25
26 261 each NWM input feature and the total performance change (NSE, bias and peak timing). These
27
28 262 correlations were calculated for different flow regimes (all flows using the whole hydrograph,
29
30 263 rising/falling limbs using the single day differentials, and high/low flows using the top 80% and
31
32 264 bottom 20%). The strengths of these correlations (positive or negative) indicated which types of
33
34 265 basins (via NWM features) are benefiting most from a LSTM post-processor. Results for rising
35
36 266 limbs and falling limbs of the hydrograph were qualitatively similar to this figure, and were
37
38 267 therefore omitted.

39
40
41
42
43 268 **Splitting the CAMELS catchments by calibrated / uncalibrated.** Of the NWM
44
45 269 calibrated basins, 480 overlap with the 531 CAMELS catchments used in this study. In a
46
47 270 separate set of experiments, we trained the LSTM_A and the LSTM post-processors LSMT_PP
48
49 271 and LSTM_PPA) on only the 480 calibrated basins. We then used the full set of 531 catchments
50
51 272 to test the performance out-of-sample. We analyzed the 480 in-sample basins and 51 out-of-
52
53 273 sample basins separately using the NSE, bias and timing error metrics. This allowed us to
54
55
56
57
58
59
60

274 determine if the LSTM is a suitable post-processing method to use in uncalibrated basins. If the
 275 post-processors trained only on calibrated basins can improve streamflow predictions at
 276 uncalibrated basins, then they would be considered suitable, particularly if there is no statistical
 277 difference between the post-processor's performance improvement over the baseline models.

278 Sensitivity analysis and NWM process diagnostics. We trained a set of LSTM post-
 279 processors using different combinations of NWM outputs as input to the LSTM, as described in
 280 Table 5. To test the sensitivity to the NWM streamflow prediction itself, we trained an LSTM
 281 with only streamflow (LSTM_Q_only), and excluded it from another (LSTM_PP_noQ). We
 282 tested the sensitivity to the channel routing (LSTM_chrt) and land surface (LSTM_ldas)
 283 components of the NWM by training LSTMs with only these dynamic inputs. These modes were
 284 trained with the same specifications as the baseline LSTM_A, LSTM_PPA and LSTM_PP.

285 TABLE 5. Additional models for sensitivity analysis and NWM diagnostics

Model label	Number of dynamic LSTM parameters	Model description
LSTM_PP_noQ	26	LSTM post-processor (LSTM_PP) but without streamflow or velocity.
LSTM_Q_only	1	LSTM trained with NWM streamflow only.
LSTM_chrt	6	LSTM trained with NWM channel routing outputs only.
LSTM_ldas	18	LSTM trained with NWM land surface outputs only.

286
 287 Each of these models, in addition to the main post-processing models presented above,
 288 have a distinct flow of information that we can use to diagnose NWM model processes. Figure 2
 289 shows the information flow of each of the model subcomponents. We used the performance
 290 results of the different post-processing models to assess how much information passes between
 291 the model components. Nearing et al., (2015) described the method to quantify the information
 292 exchange down a modeling chain (i.e., integrating over the expected effect of the conditional
 293 probability), but since we used limited outputs from the NWM reanalysis, rather than the full

state space, we examined the NWM only qualitatively for information loss between the major NWM sub-components (land surface runoff, overland router and channel router). The LSTM extracts information from its input to make predictions about its target, in our case streamflow, and we assumed higher streamflow prediction accuracy indicated more information is available in the NWM components used as input. If a post-processor made less accurate streamflow predictions than the baseline LSTM, then this indicates that information from the atmospheric forcings was lost along the NWM modeling chain.

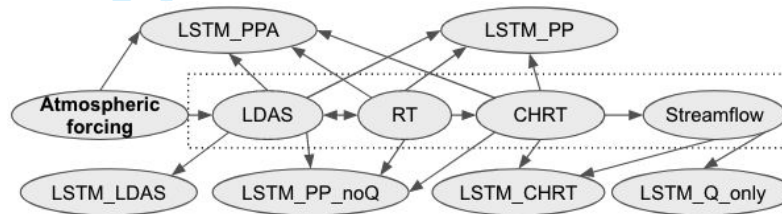


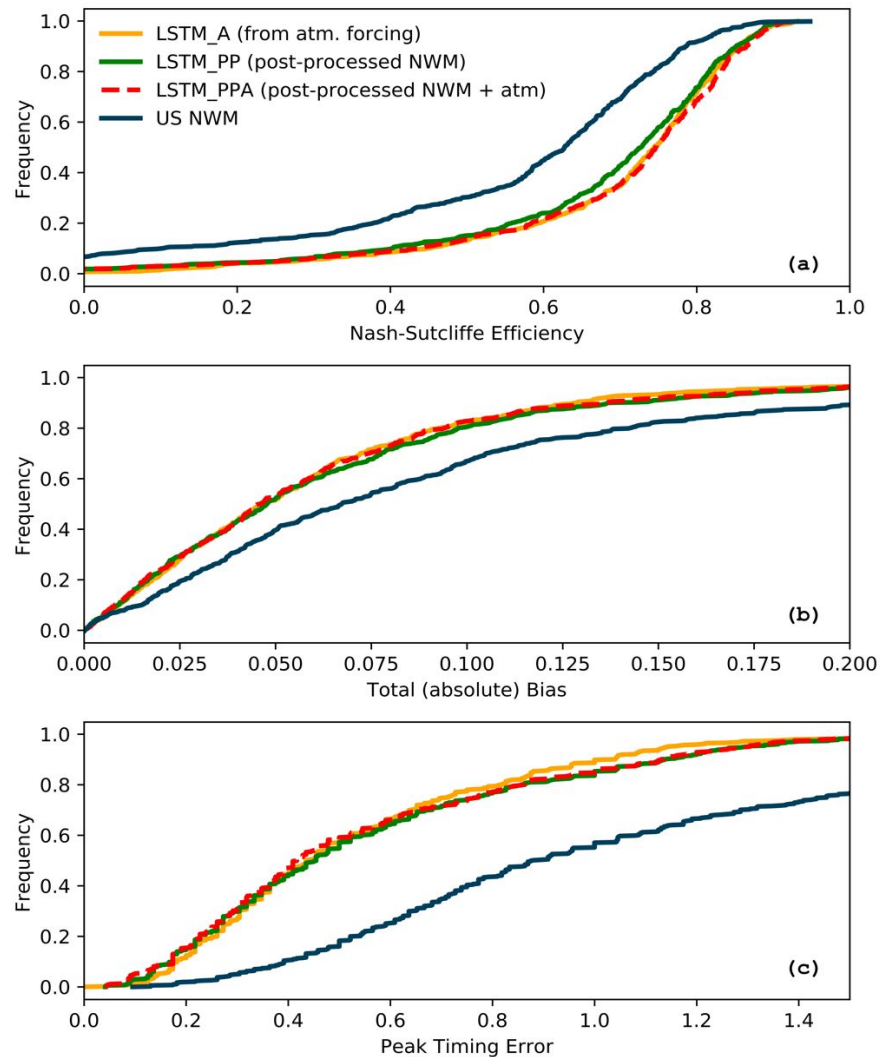
FIGURE 2. Process network diagram showing the information flow of each of these models. Arrows indicate the information flow from one component of the model to another. The NWM components are outlined with the dashed box. This is also a good guide for understanding the inputs to the different post-processing models.

RESULTS

Overall model performance

Post-processing the NWM with LSTMs significantly improved predictive performance, both with or without including the atmospheric forcings as inputs into the model. Figure 3 shows the cumulative distributions of three performance metrics (NSE, peak timing error, and total bias).

Revised manuscript submitted to the Journal of The American Water Resources Association (JAWRA) March 2021



311
312
313
314
315
316
317

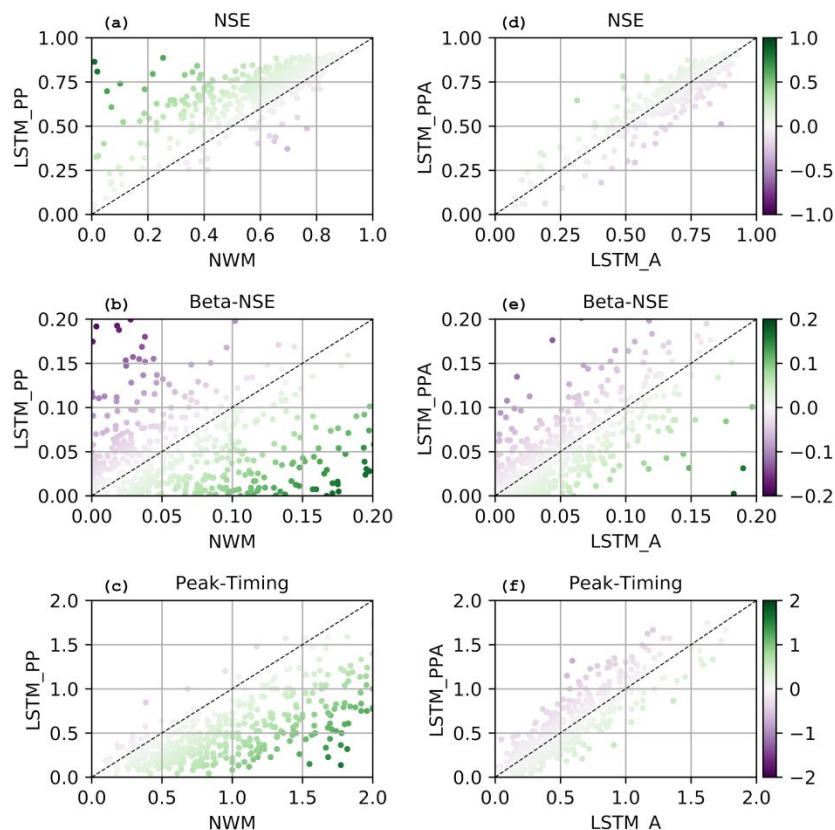
FIGURE 3. Results showing the cumulative distributions of model performance calculated as Nash-Sutcliffe Efficiency (NSE), total bias, and peak timing error over a 10-year test period in 531 CAMELS catchments. The National Water Model (NWM) reanalysis streamflow was averaged daily, long short-term memory (LSTM) networks shown used (i) the original atmospheric inputs (LSTM_A), (ii) NWM states and fluxes only (LSTM_PP), and (iii) both atmospheric forcings and NWM states and fluxes (LSTM_PPA). These figures omit the distribution tails for clarity.

318
319
320

The LSTM_PP improved the NSE score of the NWM mean daily streamflow at a total of 465 (88%) and reduced accuracy in 66 basins (12%) of the total 531 CAMELS basins, improved the total bias of the NWM mean daily streamflow at a total of 325 (61%) of basins and improved

1
2
3 321 the peak timing error at a total of 488 (92%) of basins. The LSTM_PPA post-processor improved
4
5 322 the NSE score of the NWM mean daily streamflow at a total of 488 (92%) and reduced accuracy
6
7 323 in 43 basins (8%) of the total 531 CAMELS basins. The LSTM_PPA post-processor improved
8
9 324 the total bias of the NWM mean daily streamflow at a total of 331 (62%) of basins and improved
10
11 325 the peak timing error at a total of 494 (93%) of basins. The LSTM_A (the baseline LSTM
12
13 326 without NWM states and fluxes) outperformed the NWM at a total of 473 (89%) and reduced
14
15 327 accuracy in 58 basins (11%), improved the total bias of the NWM mean daily streamflow at a
16
17 328 total of 339 basins (64%) and improved the peak timing error at a total of 484 basins (91%). The
18
19 329 LSTM_PPA improved the greatest number of basins in terms of NSE and peak timing error and
20
21 330 the LSTM_A was the best performing model in terms of total bias. Figure 4 shows scatter plots
22
23 331 of the post-processor performance at individual basins against the performance of the baseline
24
25 332 models.
26
27
28
29
30
31
32
33
34
35
36
37
38
39
40
41
42
43
44
45
46
47
48
49
50
51
52
53
54
55
56
57
58
59
60

Revised manuscript submitted to the Journal of The American Water Resources Association (JAWRA) March 2021



333

334 FIGURE 4. Performance differences of the post-processors against the baseline models (NWM and
 335 LSTM_A) in 531 CAMELS basins across CONUS. Green indicates basins where post-processing improved
 336 performance over the baseline (darker indicates larger relative improvement), and purple indicates basins where
 337 there was a decrease in performance (darker indicating worse relative detriment). The first column shows the
 338 performance difference between the LSTM_PP and the NWM. The second column shows the performance
 339 difference between the LSTM_PPA and the LSTM_A.

340 The post-processing models (LSTM_PP and LSTM_PPA) improved relative to the NWM
 341 in similar basins. The improvements of the two post-processing methods are correlated across all
 342 basins ($r^2 = 0.995$). Performance comparisons between the LSTM models and the NWM for each
 343 basin are plotted spatially in Figure 5. Notice that some of the highest NSE improvements
 344 between the LSTM_PP and the NWM are the worst NSE detriments between the LSTM_PPA
 345 and the LSTM_A, particularly in the northern plains. This indicates that although the post-

processor greatly improves the NWM, the information from the NWM at bad basins hinders the performance of the LSTM, or in other words, the NWM passes bad information to the LSTM.

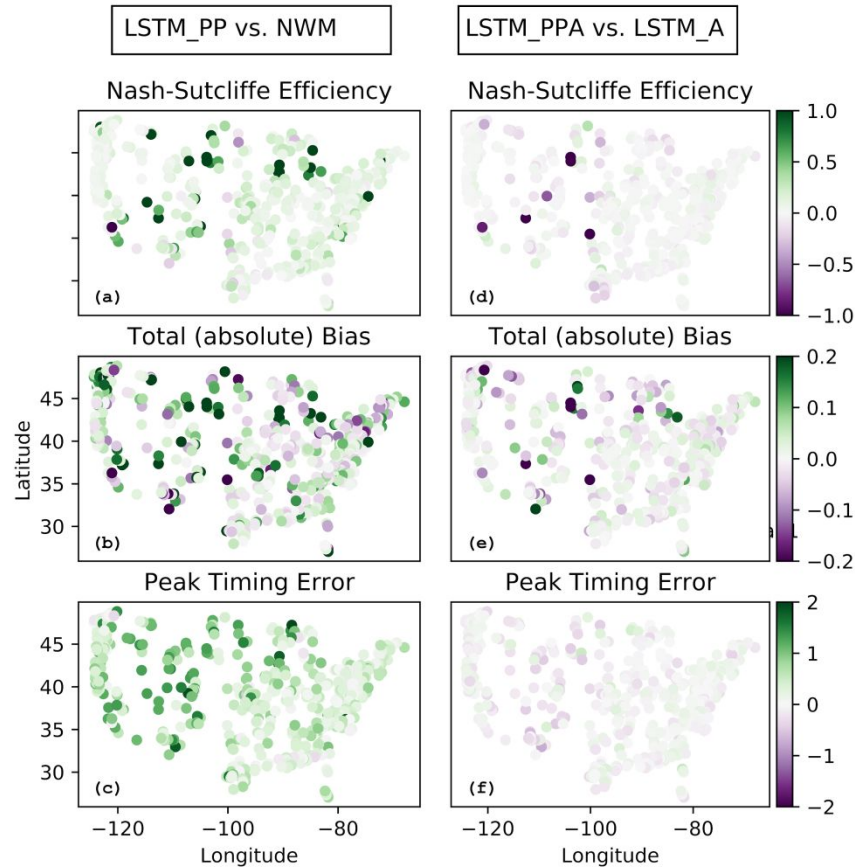


FIGURE 5. Per-basin performance change between the post-processors and baseline models (NWM and LSTM_A) in 531 CAMELS basins across CONUS. Green indicates basins where post-processing improved performance over the baseline (darker indicates larger relative improvement), and purple indicates basins where there was a decrease in performance (darker indicating worse relative detriment). The first column (a-c) shows the performance change between the LSTM_PP and the NWM. The second column (d-f) shows the performance change between the LSTM_PPA and the LSTM_A.

Performance by flow regime

Revised manuscript submitted to the Journal of The American Water Resources Association (JAWRA) March 2021

357 The LSTM post-processors improved predictive performance of the NWM according to
 358 the NSE and KGE metrics, as well as their components (variance and correlation). A full set of
 359 performance metrics broken down by flow regime are shown in Table 6. The left side of the table
 360 shows the average of metrics calculated individually at each basin, and the right side of the table
 361 shows the metrics as calculated combining the flows from all basins. The NSE includes both
 362 mean and median averages, but the rest of the metrics are only averaged by median.

363 TABLE 6. Predictive performance for NWM, LSTM_A and the LSTM Post-processors during various flow
 364 regimes. The Nash-Sutcliffe Efficiency (NSE) and Kling-Gupta Efficiency (KGE) are overall performance metrics
 365 of prediction quality. Variance, bias and correlation (R) are the components of the NSE. We calculated these in two
 366 ways: 1) at each basin and averaged across all basins, and 2) once using the observed and predicted streamflow
 367 values from all basins combined. Note that calculations done once across all basins do not include a test of
 368 significance.

Flow categories		Calculated per-basin						All basins			
All flows	NSE (mean)	NSE (median)	KGE	variance	bias	R	NSE	variance	bias	R	
NWM	0.46	0.62	0.64	0.82	-0.01 [^]	0.82	0.75	0.85	-0.02	0.87	
LSTM_PP	0.65*	0.73*	0.74*	0.86	0.02	0.87*	0.81	0.92	0.02	0.90	
LSTM_A	0.69	0.74	0.74	0.83	0.02	0.88	0.82	0.89	0.01	0.90	
LSTM_PPA	0.67	0.75	0.76	0.87	0.02	0.88	0.82	0.93	0.02	0.91	
Rising limbs	NSE (mean)	NSE (median)	KGE	variance	bias	R	NSE	variance	bias	R	
NWM	0.47	0.60	0.60	0.77	-0.07	0.81	0.73	0.82	-0.05	0.85	
LSTM_PP	0.64*	0.70*	0.72*	0.83*	0.00*	0.86*	0.78	0.88	0.00	0.88	
LSTM_A	0.66	0.71	0.72	0.80	-0.01	0.86	0.78	0.85	-0.01	0.88	
LSTM_PPA	0.65	0.72	0.74	0.85	0.00	0.87	0.79	0.89	0.00	0.89	
Falling limbs	NSE (mean)	NSE (median)	KGE	variance	bias	R	NSE	variance	bias	R	
NWM	0.29	0.62	0.64	0.94	0.03	0.83	0.78	0.90	0.00	0.88	
LSTM_PP	0.62*	0.75*	0.76*	0.95*	0.07	0.90*	0.87	0.99	0.04	0.93	
LSTM_A	0.69	0.78	0.77	0.92	0.05	0.90	0.87	0.96	0.03	0.93	
LSTM_PPA	0.65	0.77	0.77	0.94	0.05	0.90	0.87	0.98	0.03	0.93	
Above 80th percentile	NSE (mean)	NSE (median)	KGE	variance	bias	R	NSE	variance	bias	R	
NWM	0.17	0.41	0.54	0.80	-0.13	0.73	0.69	0.83	-0.10	0.84	
LSTM_PP	0.47*	0.57*	0.64*	0.82	-0.08*	0.80*	0.76	0.89	-0.04	0.90	
LSTM_A	0.53	0.58	0.67	0.81	-0.08	0.81	0.78	0.86	-0.06	0.88	

	LSTM_PPA	0.50	0.60	0.69	0.84	-0.07	0.81	0.79	0.90	-0.04	0.89
Below 20th percentile	NSE (mean)	NSE (median)	KGE	variance	bias	R	NSE	variance	bias	R	
NWM	-18384.37	-17.47	-1.96	3.79	1.89 [^]	0.36	0.37	1.31	0.22	0.81	
LSTM_PP	-6941.62*	-15.66*	-1.28*	2.84*	3.21	0.43*	0.53	1.30	0.33	0.90	
LSTM_A	-4749.68	-16.35	-1.31	2.85	3.27	0.43	0.56	1.26	0.33	0.89	
LSTM_PPA	-5147.62	-14.66	-1.24	2.85	2.87	0.43	0.58	1.28	0.30	0.90	

Note: * indicates post-processing significantly helps the NWM

Note: ^ indicates post-processing significantly hurts the NWM

369

370

371

372

373

374

375

376

377

378

379

380

381

382

383

384

In general Table 6 shows that the LSTM post-processors improved over the NWM in nearly all flow regimes according to most metrics. The LSTM_PPA also improved upon the LSTM_A in more than half the basins, and by most metrics, though not significantly. The rising limb and high flow regimes were improved by the LSTM post-processors according to every metric.

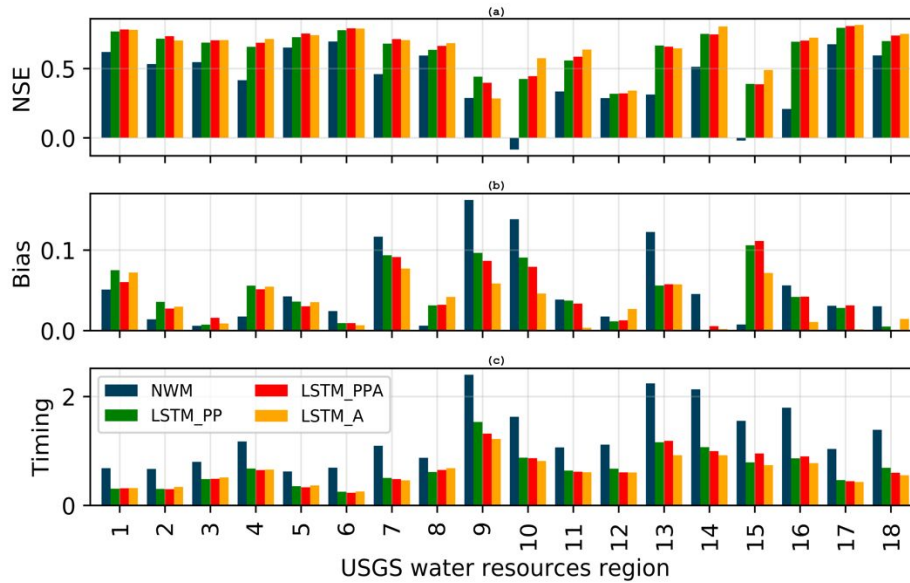
Bias was the only metric that was reduced due to post-processing, and the difference was highest in low flow regimes. Flows below the 20th percentile were poorly predicted by all models. This is likely due to the fact that all models tend to have difficulty predicting zero streamflow, and the 101 basins with periods of zero streamflow affected the average performance metrics. This will be discussed further in terms of hydrologic signatures.

The right side of the table has better performance values than the average of metrics calculated individually at each basin. This is a result of some of the better performing basins compensating for poorer performing basins, or from a different perspective, some basins have relatively poor performance which weighs down the average.

Performance by region

1
2
3 385 Results from a regional analysis of performance are shown below in Figure 6. The
4
5 386 LSTM post-processors significantly improved the NSE over the NWM in fifteen of the eighteen
6
7 387 regions, the peak timing error in sixteen regions (all regions with enough basins for a statistical
8
9 388 evaluation) and significantly improved bias in only one region. Note that region 9 was
10
11 389 represented by only two CAMELS basins, which is not sufficient for statistical evaluation. The
12
13 390 bias was better represented by the NWM than the post-processor in five of the eighteen regions,
14
15 391 including the entire East Coast (regions 1, 2 & 3), the Pacific Northwest (17) and the Lower-
16
17 392 Colorado River (15).
18
19
20
21

22 393 The regional performance of the LSTM post-processors and the regional performance of
23
24 394 the baseline LSTM_A were correlated with the regional performance of the NWM in terms of
25
26 395 NSE ($r^2=0.78$ for post-processors and 0.63 for LSTM_A) and peak timing error ($r^2=0.96$ for
27
28 396 post-processors and 0.92 for LSTM_A), but not in terms of bias ($r^2=0.24$, calculated on bias
29
30 397 although absolute bias is plotted for clarity). The post-processors and the baseline LSTM_A are
31
32 398 correlated in terms of their bias ($r^2=0.91$). A better model has a higher NSE, bias closer to zero,
33
34 399 and a lower timing error.
35
36
37
38
39
40
41
42
43
44
45
46
47
48
49
50
51
52
53
54
55
56
57
58
59
60

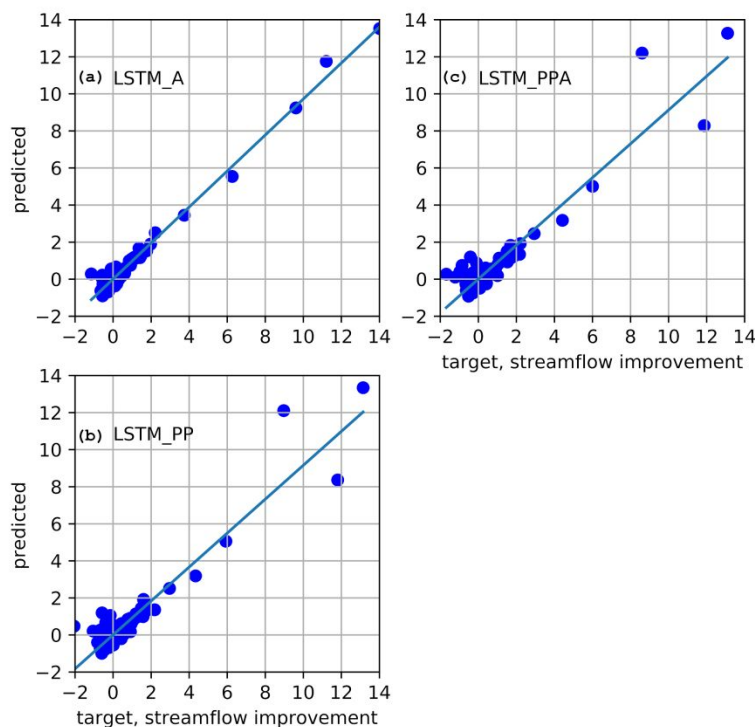


400

401 FIGURE 6. Regionally averaged performance metrics for NWM, baseline LSTM_A, and the LSTM post-processors
 402 (LSTM_PP & LSTM_PPA) in different USGS water resources regions.

403 *Regression to predict post-processing performance improvement*

404 The performance of the baseline LSTM_A was more predictable than the post-
 405 processors. We performed a linear regression on the target of performance improvement over the
 406 NWM, with inputs being the catchment attributes and hydrologic signatures, as well as the
 407 NWM performance itself. Figure 7 shows the results predicting the LSTM improvement over the
 408 NWM at each basin with an r^2 value of 0.97, 0.88 and 0.89 for the LSTM_A, LSTM_PPA and
 409 LSTM_PP, respectively. The high r^2 value is due in part to the outlier basins with abnormally
 410 large performance improvements from the LSTM models (LSTM_A, LSTM_PPA and
 411 LSTM_PP). This means that the magnitude of the baseline LSTM_A and post-processors
 412 improvement is directly related to the performance of the NWM.



413
414 FIGURE 7. Predicting LSTM (baseline and post-processor) performance over the NWM at each basin using a linear
415 regression with NWM performance and hydrologic signatures as inputs. Scatter plots with all of the 531 basins.

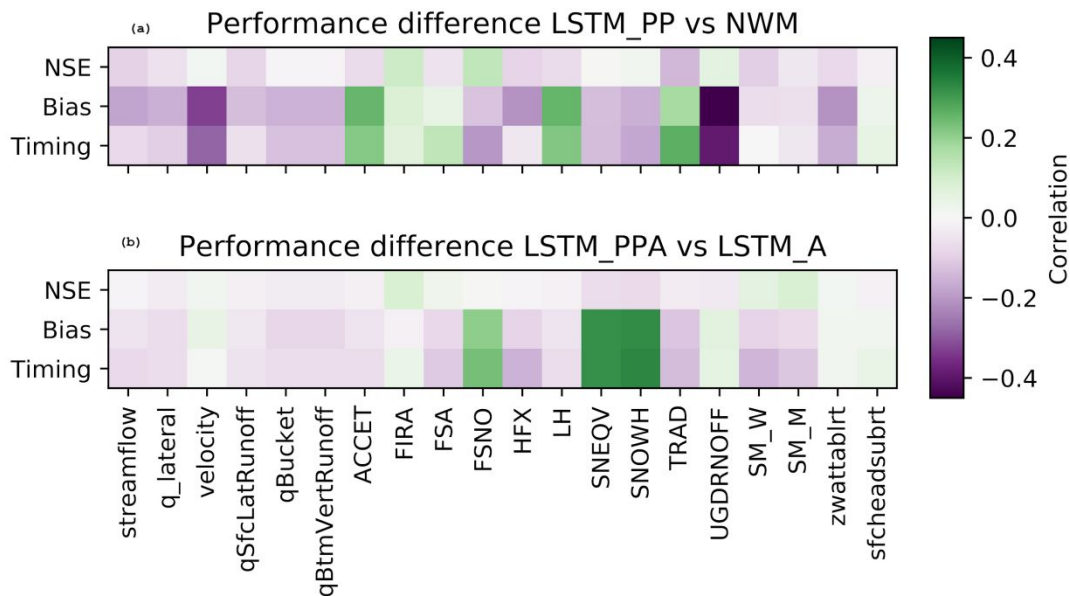
416 The aim of these results is to understand whether it is possible to predict where post-
417 processing might be beneficial (remember that post-processing helped in most basins). Although
418 we found relatively high predictability in the improvement expected from post-processing, a
419 problem is that this requires knowing ahead of time the NWM performance. This prevents us
420 from predicting post-processing improvement in *ungauged* basins, since calculating the NWM
421 performance requires streamflow observations. The correlation analysis below may help inform
422 future efforts to learn general patterns of post-processor improvement over both the NWM and the
423 baseline LSTM_A.

424

1
2
3 425 *Correlations between NWM inputs and improvements*
4
5

6 426 Figure 8 shows correlations (over 531 basins) between the time-averaged NWM inputs
7
8 427 and changes in performance metric scores of the post-processor relative to the baseline models.
9
10 428 The LSTM_PP was compared against the NWM and the LSTM_PPA was compared against the
11
12 429 LSTM_A, although qualitatively both post-processor models were similar. The rows of this
13
14 430 figure show that correlation was weaker for differences in NSE score than total bias and peak
15
16 431 timing error. Performance differences between the NWM and the post-processor were most
17
18 432 strongly (anti)correlated with stream velocity from the channel router and accumulated
19
20 433 underground runoff from the land surface model component: basins with lower stream velocity
21
22 434 (velocity) and less underground runoff (UGDRNOFF) saw greater performance improvement
23
24 435 from (daily) post-processing. This means that in basins with high underground runoff and/or high
25
26 436 stream velocity the post-processor improvements were smaller. In contrast, basins with higher
27
28 437 total radiation (TRAD) and higher latent heat flux (LH) saw greater improvement due to post-
29
30 438 processing. This means that in basins with more radiation and heat flux the post-processor
31
32 439 improvements were larger. A direct interpretation of this could be that a flat meandering stream
33
34 440 in the Southwest will benefit from post-processing, which is consistent with the findings of Salas
35
36 441 et al. (2018) that WRF-Hydro's performance is generally poor in the Southwest. Performance
37
38 442 differences between the baseline LSTM_A and the post-processor were most strongly correlated
39
40 443 with snow water equivalent and snow depth. This is consistent with the findings of Hansen et al.
41
42 444 (2019) that the NWM represents snowpack hydrology well.
43
44
45
46
47
48
49
50
51
52
53
54
55
56
57
58
59
60

Revised manuscript submitted to the Journal of The American Water Resources Association (JAWRA) March 2021

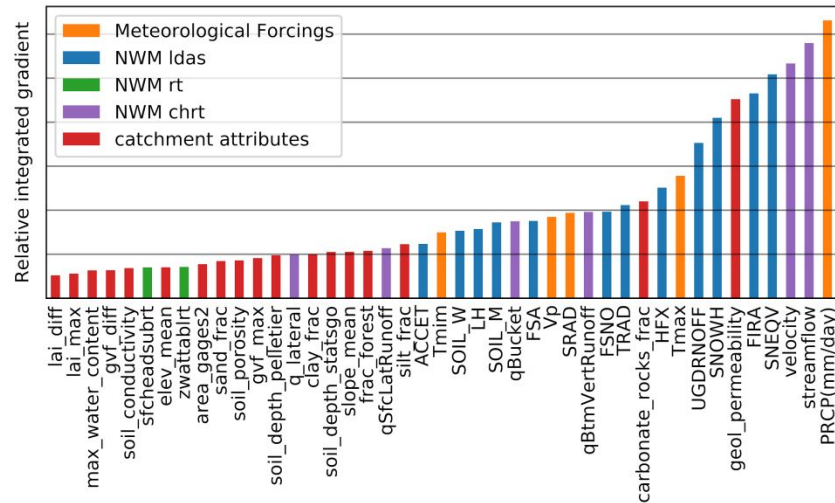


445
446 FIGURE 8. Correlations between the time-averaged NWM related inputs vs. performance metric differences
447 between the LSTM post-processors (LSTM_PP & LSTM_PPA) and baseline models (NWM & LSTM_A).

448 *Integrated gradients*

449 Figure 9 shows the relative strength of the total attribution of the dynamic inputs to the
450 LSTM_PPA averaged across the entire validation period and across basins. The ordered
451 magnitudes of the integrated gradients can be interpreted as corresponding to the order of
452 importance of inputs. The most important dynamic features for the LSTM_PPA were: (i)
453 precipitation from NLDAS, and (ii) routed streamflow from the NWM point data. Precipitation
454 inputs were weighted higher than the NWM streamflow output itself, which means that even
455 when NWM streamflow data were available, the LSTM_PPA generally learned to get
456 information directly from forcings rather than from the NWM streamflow output. This indicates
457 that the LSTM_PPA generated a new rainfall-runoff relationship rather than relying on the

458 NWM, which is consistent with the overall results (Figure 2) that showed similar performance
 459 between the LSTM_A and LSTM_PPA.



460
 461 FIGURE 9. Attributions to the LSTM_PPA predictions. The vertical axis shows the relative magnitude of attribution
 462 (importance) for each input, with precipitation (PRCP) as the top contributor and NWM-predicted runoff into
 463 channel reach ($q_{lateral}$) contributing the least.

464 Figure 10 shows the relative strength of the total attribution of the dynamic inputs to the
 465 LSTM_PP. Without the atmospheric forcings included in the post-processor inputs the NWM
 466 streamflow output was by far the highest contributing dynamic input feature to the LSTM_PP.
 467 The static permeability of the catchment was the next highest.

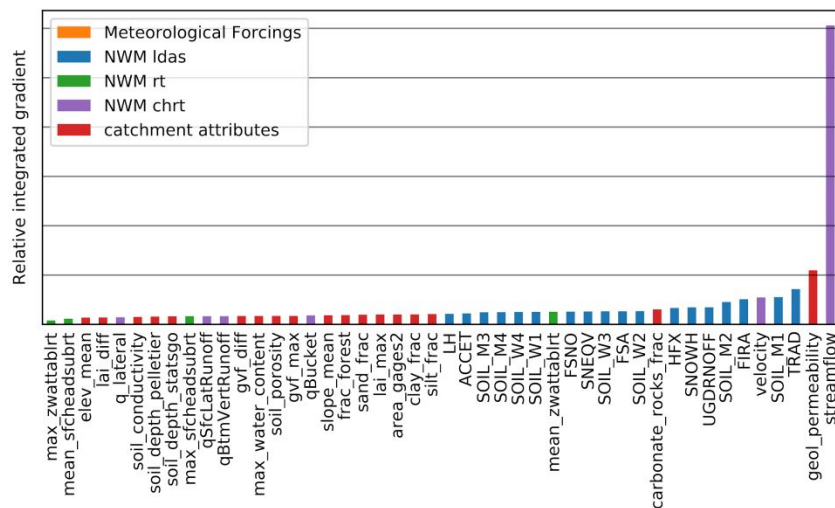
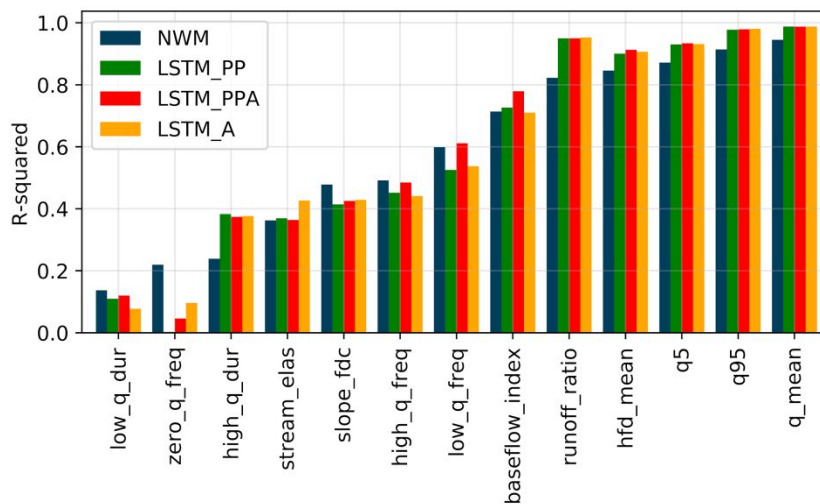


FIGURE 10. Attributions for the LSTM_PP model. Color coded by LSTM input source. The streamflow is overwhelmingly the highest contributor to the post-processed streamflow prediction.

Representations of hydrologic signatures

Results of the analysis of hydrologic signature representation are shown in Figure 11, which also shows that the hydrologic signatures best represented by the NWM were similarly those best represented by the LSTM_PPA. The same was true for the most poorly represented hydrologic signatures in both models.



476

1
2
3 477 FIGURE 11. Correlation between simulated and observed per-basin hydrologic signatures from the NWM (blue),
4
5 478 LSTM_A (orange), LSTM_PPA (green), and LSTM_PP (red). Larger values indicates better performance..
6

7
8 479 The LSTM post-processors hurt the representation of the frequency of days with zero
9
10 480 flow. There were 101 basins with any periods of zero flow. None of these models do well
11
12 481 simulating zero flow, but the NWM is better at handling this situation, predicting zero flow
13
14 482 periods in 56 of the 101 basins. The LSTM_A, LSTM_PPA and LSTM_PP only predicted
15
16 483 periods of zero flows at 35, 29 and 25 basins, respectively. This is an important characteristic in
17
18 484 basins in the Southwest, where the NWM could use the benefit of a LSTM post-processor, so
19
20 485 this would be a good place to focus future research of theory-guided ML for hydrology.
21
22
23

24 486 The LSTM post-processor made a significant improvement over the NWM for several
25
26 487 signatures. The improvement to runoff ratio, which is the fraction of precipitation that makes it
27
28 488 through the stream gauge at the surface, could be a compensation for the uncalibrated soil
29
30 489 parameters in the NWM mentioned by Salas *et al.* (2018). The LSTM post-processor improved
31
32 490 both high and low flow predictions (5% & 95% flow quantiles), which are important for natural
33
34 491 resources management. Mean daily discharge was the best represented hydrologic signature by
35
36 492 all models.
37
38
39
40

41 493 The LSTM_PPA post-processor made significant improvements over the LSTM for
42
43 494 baseflow index. This is the only signature that an LSTM post-processor improved over both the
44
45 495 NWM and the baseline LSTM_A. This signature estimates the contribution of baseflow to the
46
47 496 total discharge, which is computed by hydrograph separation. Klemeš (1986) (summarizing
48
49 497 Lindsly's Applied Hydrology) cautioned strongly against using hydrograph separation, because
50
51 498 there is no real basis for distinguishing the source of flow in a stream.
52
53
54
55

56 499 *Results comparing gauged basins vs. ungauged basins*
57
58
59
60

500 Results in Table 9 summarize an analysis designed to replicate prediction in ungauged
 501 basins. The table has metrics from predictions by the NWM, LSTM_A and the LSTM post-
 502 processors (LSTM_PP & LSTM_PPA) calculated only at basins that were either calibrated or
 503 uncalibrated, but not both. There was no statistical difference between the calibrated and
 504 uncalibrated samples. This indicates that the LSTM post-processor works in uncalibrated basins.
 505 When post-processors were trained only in calibrated basins (denoted with a “C” in Table 9),
 506 however, the performance in uncalibrated basins significantly deteriorated. But this is true for the
 507 baseline LSTM_A as well, so it is not a result of the calibration (as calibration would not
 508 influence the baseline LSTM_A), but a result of prediction at ungauged type basins. However,
 509 the median performance of the post-processor predictions at ungauged type basins when trained
 510 at only calibrated basins was still better significantly than the NWM in the uncalibrated basins.

511 TABLE 9. Performance of the LSTM and the LSTM post processor split between basins where the NWM was
 512 calibrated vs. uncalibrated. The “C” in the model name denotes that the model was trained only on calibrated basins

Nash-Sutcliffe Efficiency									
	Calibrated basins				Uncalibrated basins				
	mean	median	max	min	mean	median	max	min	
NWM	0.49	0.64	0.95	-10.81	0.18	0.48	0.79	-7.10	
LSTM_PP	0.65	0.73	0.93	-3.32	0.69	0.71	0.89	0.38	
LSTM_A	0.68	0.74	0.93	-0.64	0.73	0.75	0.89	0.43	
LSTM_PPA	0.66	0.75	0.93	-3.61	0.71	0.73	0.89	0.42	
LSTM_PP(C)	0.65	0.73	0.93	-1.86	0.21	0.57	0.75	-8.12	
LSTM_A(C)	0.67	0.74	0.93	-1.13	0.51	0.67	0.84	-2.54	
LSTM_PPA(C)	0.67	0.75	0.94	-2.71	0.13	0.58	0.84	-14.07	
Total bias									
	Calibrated basins				Uncalibrated basins				
	mean	median	max	min	mean	median	max	min	

NWM	0.01	-0.01	2.57	-0.63	0.00	-0.06	1.84	-0.58	
LSTM_PP	0.04	0.02	1.05	-0.24	0.02	0.01	0.27	-0.12	
LSTM_A	0.02	0.02	0.56	-0.22	0.02	0.01	0.20	-0.11	
LSTM_PPA	0.03	0.02	0.98	-0.21	0.01	0.00	0.22	-0.11	
LSTM_PP(C)	0.01	-0.01	0.92	-0.25	0.06	-0.04	2.15	-0.51	
LSTM_A(C)	0.02	0.02	0.62	-0.21	0.09	0.04	0.99	-0.20	
LSTM-PPA(C)	0.01	0.00	0.95	-0.22	0.06	-0.05	2.89	-0.41	
Peak timing error									
	Calibrated basins				Uncalibrated basins				
	mean	median	max	min	mean	median	max	min	
NWM	1.06	0.91	3.00	0.10	1.04	0.77	2.70	0.25	
LSTM_PP	0.55	0.45	1.95	0.04	0.52	0.35	1.59	0.04	
LSTM_A	0.53	0.43	1.76	0.00	0.51	0.41	1.50	0.04	
LSTM_PPA	0.54	0.42	1.75	0.04	0.51	0.36	1.45	0.05	
LSTM_PP(C)	0.55	0.45	2.10	0.00	0.59	0.41	1.76	0.09	
LSTM_A(C)	0.52	0.43	1.77	0.00	0.57	0.50	1.50	0.08	
LSTM_PPA(C)	0.54	0.41	1.83	0.04	0.57	0.41	1.65	0.13	

513

514 The NWM, LSTM_A and the LSTM_PPA had higher NSE scores in calibrated basins

515 than the uncalibrated basins. Note that these results are from the LSTMs (baseline and post-

516 processors) trained on only basins where the NWM was calibrated. In the case of the LSTM

517 post-processors the mean NSE scores in uncalibrated basins were very low for NSE. This is a

518 result of two outlier basins (1466500, MCDONALDS BRANCH, Lat:39.9, Lon:-74.5, Area:

519 5.7km²; and 01484100 BEAVERDAM BRANCH, Lat:38.9, Lon:-75.5, Area: 7.8km²). Both of

520 those outlier basins are much smaller, and have lower flows, than what were included in the

521 training set. Without these basins the mean NSE scores were 0.32, 0.51, 0.56 and 0.56 for the

1
2
3 522 NWM, LSTM_PP, LSTM_A and LSTM_PPA, respectively. Table 9 also shows that the median
4
5 523 value of the LSTM_PPA was higher than the NWM, as was the maximum NSE value, but the
6
7 524 minimum value was exceptionally low.

8
9
10 525 The total bias in calibrated basins was generally better (lower) than the uncalibrated
11
12 526 basins. The timing error of the NWM was actually better in the uncalibrated basins, but the
13
14 527 LSTM_A and LSTM post-processors had better performance in the calibrated basins. The NSE
15
16 528 values for the NWM, LSTM_A and the LSTM post-processors (LSTM_PP and LSTM_PPA)
17
18 529 were significantly different in the calibrated basins vs. the uncalibrated basins, as were the
19
20 530 differences between the LSTM_A and LSTM post-processors (LSTM_PP and LSTM_PPA)
21
22 531 compared to the NWM. The bias values were significantly different between the two samples
23
24 532 (calibrated vs. uncalibrated), but the differences between LSTM_A and LSTM post-processors
25
26 533 vs. the NWM were not statistically different. This means that the LSTM models were successful
27
28 534 at predicting streamflow at basins outside of the calibration set.

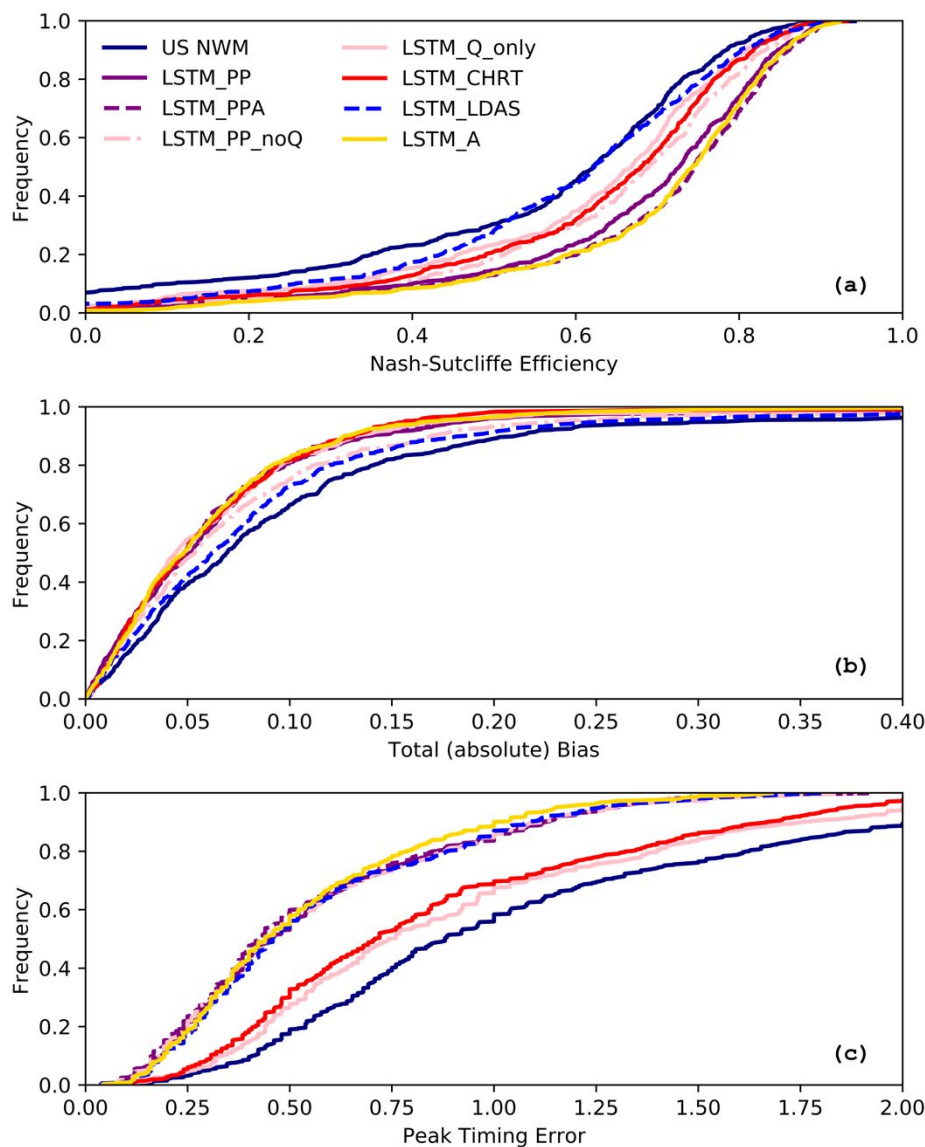
29
30
31
32
33
34 535 *LSTM post-processor sensitivity to inputs and application for process representation*
35
36 536 *diagnostics.*

37
38
39
40 537 Figure 12 shows results from the LSTM models with inputs from different parts of the
41
42 538 NWM (land surface model only, channel router only, predicted streamflow only, and all states
43
44 539 and fluxes. The best performing LSTM models (LSTM_A & LSTM_PPA) were the ones trained
45
46 540 with inputs that included the five atmospheric forcing variables with (LSTM_PPA) and without
47
48 541 (LSTM_A) the NWM output (these are the same models discussed in previous sections above).
49
50 542 This implies that LSTM in general was able to extract more information from the atmospheric
51
52 543 forcings than the NWM. Each of the LSTM post-processors made better average daily
53
54 544 streamflow predictions than the NWM itself, indicating that information from the atmospheric
55
56
57
58
59
60

1
2
3 545 forcings is lost in the NWM model structure before the streamflow prediction is made. For
4
5 546 example, the LSTM that took as inputs only the LDAS model output from the NWM made better
6
7 547 predictions than the NWM itself, indicating that there is more information in the LDAS states
8
9 548 and fluxes than the NWM is able to translate into streamflow predictions. The same was true for
10
11 549 the states and fluxes of the CHRT component of the NWM, meaning that information is also lost
12
13 550 in the CHRT component of the NWM model structure.
14
15
16
17
18 551

19
20
21
22
23
24
25
26
27
28
29
30
31
32
33
34
35
36
37
38
39
40
41
42
43
44
45
46
47
48
49
50
51
52
53
54
55
56
57
58
59
60

For Peer Review



552

553 FIGURE 12. Performance of the LSTM post-processor trained with different sets of NWM output. Each of
 554 these post-processors outperform the NWM. LSTM_A is the baseline LSTM trained with atmospheric forcings as
 555 dynamic inputs. LSTM_PP is the NWM post-processor trained with the outputs of the NWM as dynamic inputs.
 556 LSTM_PPA used both the NWM outputs and atmospheric forcings as inputs. LSTM_PP_noQ used all the NWM
 557 outputs except for streamflow and velocity from the channel router. LSTM_Q_only used only streamflow from the
 558 NWM output. LSTM_chrt used only the NWM channel router outputs. LSTM_ldas used only the land surface
 559 fluxes as inputs.

DISCUSSION

Comparison between the baseline LSTM and the post-processors

The baseline LSTM (LSTM_A), trained only on atmospheric forcings as dynamic inputs, was better at extrapolating hydrologic conditions outside the training set than the LSTM post-processors (LSTM_PP & LSTM_PPA). This is shown in the analysis of prediction in ungauged basins, specifically Table 9. The post-processors both failed to make reasonable predictions at two basins that were much smaller than any basins included in the training set. The LSTM_A was able to make good predictions in these basins. Including the NWM output as dynamic inputs to the LSTM constrained the model and prevented it from learning general hydrologic relationships that can be extracted to basins with characteristics that might be unrecognizable.

Potential for improving the performance of both the National Water Model and machine learning

Results presented here show that the LSTM post-processors have potential to improve the daily averaged flow predictions of the NWM. The LSTM post-processors provided significant benefit to the NWM streamflow predictions at almost all (88% & 92% for LSTM_PP & LSTM_PPA, respectively) of the 531 basins analyzed here. In the few basins where this was not the case, it may be possible to use fine tuning a version of the post-processor that is specific to each gauge location (as would be done in traditional model calibration), however the LSTM post-processors used here can be applied to any basin, even ungauged. The post-processors were trained on headwater basins, so further work would be needed to include reservoirs and other management practices. It is worth noting that these LSTM models can be trained on a laptop computer in a few hours, a relatively minor computational cost, and the computational cost of

1
2
3 582 forward prediction is negligible. By comparison the computational cost of calibrating the NWM
4
5 583 is much higher - typically requiring HPC or cloud systems.
6
7

8 584 The NWM performance and the performance improvement from the LSTM post-
9
10 585 processors (LSTM_PP & LSTM_PPA) were negatively correlated: basins with low performance
11
12 586 by the NWM have the highest performance change from the LSTM post-processors. This means
13
14 587 that post-processing can be expected to correct situations where the NWM gives bad predictions.
15
16 588 Conversely, the performance of the NWM and the LSTM_A (the baseline LSTM without NWM
17
18 589 inputs) were minimally correlated (r-squared = 0.42, 0.30 and 0.67 for NSE, bias and timing,
19
20 590 respectively). Considering also that the overall performance of the LSTM_A changed only
21
22 591 minimally from the addition of the NWM inputs (as shown in Figures 3-5 and Table 6) and that
23
24 592 the LSTM_PPA still preferred to extract more information from precipitation forcings (shown in
25
26 593 Figure 9), we might conclude that the LSTM post-processors learned new patterns of the rainfall-
27
28 594 runoff response, which are not fully represented by the NWM. The overall improvement in the
29
30 595 representation of hydrologic signatures indicates this new rainfall-runoff response is a better
31
32 596 representation of physical flow patterns than either the NWM or the LSTM_A. The interpretation
33
34 597 of the integrated gradient (Figures 9 & 10) and the correlations between improvement and NWM
35
36 598 features (Figure 8) indicate that this improvement of flow patterns comes from information in the
37
38 599 NWM representation of streamflow and snow states.
39
40
41
42
43
44
45

46 600 *Application to real-time forecasting*

47
48

49 601 The NWM is not simply a rainfall-runoff simulator; it simulates flow through 2.7 million
50
51 602 river reaches around CONUS, dam operations, land surface processes, hydraulics, and other
52
53 603 complications of large domain hydrology. The nature of the CAMELS catchments selected in
54
55 604 these experiments are such that they have few engineered control structures, and are under
56
57
58
59
60

1
2
3 605 20,000 km². The results presented in this paper show that the LSTM post-processors improved
4
5 606 streamflow predictions in the catchments studied here, which all had limited human disturbance
6
7 607 (e.g., dams, reservoirs, *etc.*). Kratzert *et al.* (2019) showed that these predictions extend into
8
9 608 ungauged basins. Our results (section “*Results comparing calibrated basins vs. uncalibrated*
10
11 609 *basins*”) show that this is true for all but the poorest performing NWM basins. The immediate
12
13 610 potential for improving real-time forecasting could be deploying an LSTM for streamflow
14
15 611 prediction in undisturbed catchments, and undisturbed sub-catchments upstream of unnatural
16
17 612 hydrologic conditions such as dams, agriculture lands and urban centers. This would allow for
18
19 613 retaining conceptual representations of lakes and reservoirs that already exist in the NWM.
20
21
22
23

24 614 *Diagnosing process-based models, physical processes and data concerns*

25
26
27 615 The sensitivity analysis reported in Figure 12 showed that some components of the NWM
28
29 616 caused poor predictions. Specifically, information was lost in channel router (CHRT) component
30
31 617 of the model. This diagnostic method could be used to compare different schemes for future
32
33 618 versions of the NWM. For instance, changing the routing function might conserve timing
34
35 619 information from the land surface fluxes, or modifying the evapotranspiration options in Noah-
36
37 620 MP may conserve mass bias information from the NWM forcing engine. Such improvements
38
39 621 could be quantified with this post-processing method.
40
41
42
43

44 622 Each of the post-processing models tested for sensitivity (Figure 12) fall, roughly and
45
46 623 inclusively, between the NWM and the baseline LSTM_A. Based on the relative positions
47
48 624 between those bounding curves, we can identify sources of information loss through the NWM
49
50 625 modeling chain:
51
52
53
54
55
56
57
58
59
60

- 1
2
3 626 • The channel routing outputs contain more information of simulation bias than
4
5 627 timing, meaning the channel router moves with poor timing, but conserves mass
6
7 628 well.
8
9
10 629 • The land surface outputs contain more information of simulation timing than bias,
11
12 630 meaning the land surface component does not conserve mass well, but delivers
13
14 631 water to the channel at appropriate times.
15
16
17 632 • Information is lost during channel routing after the mass is delivered, indicating
18
19 633 the channel router is not functioning properly.
20
21

22 634 There is potential to expand this analysis, breaking down the NWM components even further.
23
24 635 Quantification can be done with the full state space from the NWM. Retrospective runs using
25
26 636 new versions of the NWM should output the full state space for these types of analysis. This
27
28 637 diagnostics analysis using ML post-processing is possible with any physics-based, conceptual or
29
30 638 process-based dynamics model.
31
32

33
34
35 639 *Moving forward with theory-guided machine learning*
36

37
38 640 The post-processing procedure presented here is one of the cruder techniques currently
39
40 641 available for combining process-based and data-driven models. Several other methods of
41
42 642 combining the benefits of machine learning (predictability) with the benefits of physically
43
44 643 realistic hydrologic theory (robustness) are in development. For example, Pelissier *et al.* (2019)
45
46 644 integrated a trained Gaussian Processes into the state-space dynamics of a process-based land
47
48 645 surface model for predicting soil moisture time series. Another example is using physical
49
50 646 principles to constrain the loss function of an ML model during training - for example Hoedt *et*
51
52 647 *al.* (2020) integrated mass balance constraints into an LSTM and applied this model to the same
53
54 648 531 basins used in this study. Implementing post-processing is relatively straightforward
55
56
57
58
59
60

649 compared to other techniques such as adding physics into ML code or using ML to dynamically
650 update the state variables.

651 Using ML for post-processing has potential for advancing the explainability of data-
652 driven models. We showed that the LSTM model representation of hydrologic signatures (post-
653 processed and baseline) is highly correlated with the NWM. This indicates that the “learned”
654 functions mapping inputs to streamflow are actually quite similar. We might have trouble
655 expressing the “learned” LSTM with compact formulas (e.g., PDEs), given the high number of
656 trained model weights, but we can use them with confidence knowing their structural similarities
657 with process-based models like the NWM.

658 CONCLUSION

659 The LSTM post-processors (LSTM_PPA & LSTM_PP) significantly outperformed the
660 NWM, but only slightly outperformed the LSTM_A (the baseline LSTM without the NWM
661 states and fluxes as inputs). LSTMs, in general, are capable of learning the dynamics of rainfall-
662 runoff processes, gaining little additional information from the conceptualizations coded within
663 the NWM. The “pure” post-processing model (LSTM_PP) outperformed the NWM in terms of
664 bias, and significantly outperformed the NWM in terms of NSE and timing. A decision to use the
665 LSTM as a post-processor for the NWM should be made with professional judgement,
666 considering the comparison of the NWM, LSTM and LSTM post-processor’s performance. In
667 locations where the NWM is not calibrated, or the hydrologic conditions are not well understood,
668 it would be best to use the LSTM without the influence from the NWM.

669 The results indicate that there is more information in the atmospheric forcings about
670 streamflow observations than in the NWM outputs, including the NWM streamflow prediction.

1
2
3 671 The NWM loses information between the atmospheric forcing inputs and the outputs. The NWM
4
5 672 land surface component (LDAS) loses information about mass conservation (shown from the
6
7
8 673 bias error), and the channel router (CHRT) loses information about streamflow timing. The
9
10 674 NWM routing scheme should be considered as a priority for improving the NWM.
11
12

13 675 DATA AVAILABILITY

14
15
16 676 All data and code used in this paper are publicly available in the following locations:
17
18 677 **U.S. National Water Model:** <https://docs.opendata.aws/nwm-archive/readme.html>
19
20 678 **CAMELS data:** <https://ral.ucar.edu/solutions/products/camels>
21
22 679 **Data processing code:** <https://github.com/jmframe/nwm-reanalysis-model-data-processing>,
23 680 DOI: 10.5281/zenodo.4642605
24
25 681 **LSTM code:** https://github.com/kratzert/ealstm_regional_modeling
26
27 682 **Post-processing and analysis code:** [https://github.com/jmframe/nwm-post-processing-with-](https://github.com/jmframe/nwm-post-processing-with-lstm)
28 683 [lstm](https://github.com/jmframe/nwm-post-processing-with-lstm), DOI: 10.5281/zenodo.4642603
29

30 684

31 685 ACKNOWLEDGEMENTS

32
33
34
35 686 Authors from Johannes Kepler University were partially supported by a Google faculty research
36
37 687 award. Jonathan Frame from the University of Alabama supported by the NASA Terrestrial
38
39 688 Hydrology Program. Grey Nearing (then at the University of Alabama) was partially supported
40
41 689 by the NCAR COMET program on a cooperative award with the National Water Center. The
42
43
44 690 LSTM models presented here were trained using computational resources from the NASA
45
46 691 Center for Climate Simulation. We thank the reviewers for their valuable feedback and
47
48
49 692 constructive criticism throughout the review of this paper.
50

51 693 LITERATURE CITED

- 1
2
3 694 Addor, N., A.J. Newman, N. Mizukami, and M. P. Clark, 2017. The CAMELS Data Set:
4
5 695 Catchment Attributes and Meteorology for Large-Sample Studies. *Earth Syst. Sci* 21:
6
7 696 5293–5313. <https://doi.org/10.5194/hess-21-5293-2017>.
9
10
11 697 Addor, N., G. Nearing, C. Prieto, A. J. Newman, N. Le Vine, and M. P. Clark, 2018. A
12
13 698 Ranking of Hydrological Signatures Based on Their Predictability in Space. *Water*
14
15 699 *Resources Research* 54, no. 11: 8792–8812. <https://doi.org/10.1029/2018WR022606>.
17
18 700 Chadalawada, J., H. M.V.V. Herath, and V. Babovic, 2020. Hydrologically Informed
19
20 701 Machine Learning for Rainfall-Runoff Modeling: A Genetic Programming-Based
21
22 702 Toolkit for Automatic Model Induction. *Water Resources Research* 56, no. 4: 1–23.
23
24 703 <https://doi.org/10.1029/2019WR026933>.
26
27
28 704 Cosgrove, B, D. Gochis, E. P. Clark, Z. Cui, A. L. Dugger, G. M. Fall, X. Feng, M. A.
29
30 705 Fresch, J. J. Gourley, S. Khan, D. Kitzmiller, H. S. Lee, Y. Liu, J. L. McCreight, A. J.
31
32 706 Newman, A. Oubeidillah, L. Pan, C. Pham, F. Salas, K. M. Sampson, M. Smith, G.
33
34 707 Sood, A. Wood, D. N. Yates, W. Yu and Y. Zhang, 2015. Hydrologic Modeling at the
35
36 708 National Water Center: Operational Implementation of the WRF-Hydro Model to
37
38 709 Support National Weather Service Hydrology. In AGU Fall Meeting Abstracts.
40
41
42
43 710 Daw, A., R. Q. Thomas, C. C. Carey, J. S. Read, A. P. Appling, and Anuj Karpatne, 2020.
44
45 711 Physics-Guided Architecture (PGA) of Neural Networks for Quantifying Uncertainty
46
47 712 in Lake Temperature Modeling. *Proceedings of the 2020 SIAM International*
48
49 713 *Conference on Data Mining*, 532–40. <https://doi.org/10.1137/1.9781611976236.60>.
50
51
52
53
54
55
56
57
58
59
60

Revised manuscript submitted to the Journal of The American Water Resources Association (JAWRA) March 2021

- 1
2
3 714 Elmer, N. J, 2019. Using Satellite Observations of River Height and Vegetation To Improve
4
5 715 National Water Model Initialization and Streamflow Prediction. PhD diss., The
6
7 716 University of Alabama in Huntsville.
8
9
10
11 717 Gauch, M., J. Mai, and J. Lin, 2019. The Proper Care and Feeding of CAMELS: How
12
13 718 Limited Training Data Affects Streamflow Prediction 2342: 0–2.
14
15 719 <http://arxiv.org/abs/1911.07249>.
16
17
18 720 Gauch, Martin, Frederik Kratzert, Daniel Klotz, Grey Nearing, Jimmy Lin, and Sepp
19
20 721 Hochreiter. 2020. Rainfall-Runoff Prediction at Multiple Timescales with a Single
22
23 722 Long Short-Term Memory Network, 2020, 1–24. <http://arxiv.org/abs/2010.07921>.
24
25
26 723 Gupta, H. V., T. Wagener, and Y. Liu, 2008. Reconciling Theory with Observations:
27
28 724 Elements of a Diagnostic Approach to Model Evaluation. *Hydrological Processes*
29
30 725 2274, no. November 2008: 2267–74. <https://doi.org/10.1002/hyp.6989>.
31
32
33
34 726 Gupta, H. V., H. Kling, K. K. Yilmaz, and G. F. Martinez, 2009. Decomposition of the
35
36 727 Mean Squared Error and NSE Performance Criteria: Implications for Improving
37
38 728 Hydrological Modelling. *Journal of Hydrology* 377, no. 1–2: 80–91.
39
40 729 <https://doi.org/10.1016/j.jhydrol.2009.08.003>.
41
42
43
44 730 Hansen, C., J. S. Shiva, S. McDonald, and A. Nabors, 2019. Assessing Retrospective
45
46 731 National Water Model Streamflow with Respect to Droughts and Low Flows in the
47
48 732 Colorado River Basin. *Journal of the American Water Resources Association* 55, no. 4:
49
50 733 964–75. <https://doi.org/10.1111/1752-1688.12784>.
51
52
53
54
55
56
57
58
59
60

- 1
2
3 734 Hochreiter, S, 1991. “Untersuchungen Zu Dynamischen Neuronalen Netzen.” Doctoral
4
5 735 diss., Institut Für Informatik, Technische Universität, Munchen
6
7 736 <http://people.idsia.ch/~juergen/SeppHochreiter1991ThesisAdvisorSchmidhuber.pdf>.
8
9
10
11 737 Hochreiter, S., and J. Schmidhuber, 1997. Long Short-Term Memory. *Neural Computation*
12
13 738 9, no. 8: 1735–80. <https://doi.org/10.1162/neco.1997.9.8.1735>.
14
15
16 739 Hoedt, P. J., F. Kratzert, D. Klotz, C. Halmich, M. Holzleitner, G. Nearing, S. Hochreiter,
17
18 740 and G. Klambauer. 2021. MC-LSTM: Mass-Conserving LSTM, 2021, 1–32.
19
20 741 <http://arxiv.org/abs/2101.05186>.
21
22
23
24 742 Karpatne, A., W. Watkins, J. Read, and V. Kumar, 2017a. Physics-Guided Neural Networks
25
26 743 (PGNN): An Application in Lake Temperature Modeling.
27
28 744 <http://arxiv.org/abs/1710.11431>.
29
30
31 745 Karpatne, A., G. Atluri, J. H. Faghmous, M. Steinbach, A. Banerjee, A. Ganguly, S.
32
33 746 Shekhar, N. Samatova, and V. Kumar, 2017b. Theory-Guided Data Science: A New
34
35 747 Paradigm for Scientific Discovery from Data. *IEEE Transactions on Knowledge and*
36
37 748 *Data Engineering* 29, no. 10: 2318–31. <https://doi.org/10.1109/TKDE.2017.2720168>.
38
39
40
41 749 Kim, J., L. Read, L. E. Johnson, D. Gochis, R. Cifelli, and H. Han, 2020. An Experiment on
42
43 750 Reservoir Representation Schemes to Improve Hydrologic Prediction: Coupling the
44
45 751 National Water Model with the HEC-ResSim. *Hydrological Sciences Journal* 0, no. 0:
46
47 752 1. <https://doi.org/10.1080/02626667.2020.1757677>.
48
49
50
51 753 Klemeš, V, 1986. Dilettantism in Hydrology: Transition or Destiny? *Water Resources*
52
53 754 *Research* 22, no. 9 S: 177S-188S. <https://doi.org/10.1029/WR022i09Sp0177S>.
54
55
56
57
58
59
60

Revised manuscript submitted to the Journal of The American Water Resources Association (JAWRA) March 2021

- 1
2
3 755 Kratzert, F., D. Klotz, C. Brenner, K. Schulz, and M. Herrnegger, 2018. Rainfall–Runoff
4
5 756 Modelling Using Long Short-Term Memory (LSTM) Networks. *Hydrology and Earth*
6
7 757 *System Sciences* 22, no. 11: 6005–22. <https://doi.org/10.5194/hess-22-6005-2018>.
9
10 758 Kratzert, F., D. Klotz, M. Herrnegger, A. K. Sampson, S. Hochreiter, and G. S. Nearing,
11
12 759 2019a. Towards Improved Predictions in Ungauged Basins: Exploiting the Power of
13
14 760 Machine Learning. *Water Resources Research*, 2019WR026065.
15
16 761 <https://doi.org/10.1029/2019WR026065>.
17
18 762 Kratzert, F., D. Klotz, G. Shalev, G. Klambauer, S. Hochreiter, and G. S. Nearing, 2019b.
19
20 763 Towards Learning Universal, Regional, and Local Hydrological Behaviors via
21
22 764 Machine Learning Applied to Large-Sample Datasets. *Hydrology and Earth System*
23
24 765 *Sciences* 23, no. 12: 5089–5110. <https://doi.org/10.5194/hess-23-5089-2019>.
25
26
27
28
29
30 766 Nearing, G. S., Benjamin L. Ruddell, Martyn P. Clark, Bart Nijssen, and Christa Peters-
31
32 767 Lidard. “Benchmarking and Process Diagnostics of Land Models.” *Journal of*
33
34 768 *Hydrometeorology*, 2018, JHM-D-17-0209.1. [https://doi.org/10.1175/JHM-D-17-](https://doi.org/10.1175/JHM-D-17-0209.1)
35
36 769 [0209.1](https://doi.org/10.1175/JHM-D-17-0209.1).
37
38
39
40 770 Nearing, G. S., F. Kratzert, D. Klotz, P.J. Hoedt, G. Klambauer, S. Hochreiter, H. Gupta, S.
41
42 771 Nevo, and Y. Matias. 2020. A Deep Learning Architecture for Conservative
43
44 772 Dynamical Systems: Application to Rainfall-Runoff Modeling. *AI for Earth Sciences*
45
46 773 *Workshop at NEURIPS 2020*, 2020.
47
48
49
50 774 Newman, A. J., M. P. Clark, K. Sampson, A. Wood, L. E. Hay, A. Bock, R. J. Viger, D.
51
52 775 Blodgett, L. Brekke, J. R. Arnold, T. Hopson, and Q. Duan, 2015. Development of a
53
54 776 Large-Sample Watershed-Scale Hydrometeorological Data Set for the Contiguous
55
56
57
58
59
60

- 1
2
3 777 USA: Data Set Characteristics and Assessment of Regional Variability in Hydrologic
4
5 778 Model Performance. *Hydrology and Earth System Sciences* 19, no. 1: 209–23.
6
7
8 779 <https://doi.org/10.5194/hess-19-209-2015>.
9
10
11 780 National Oceanic and Atmospheric Administration (NOAA). 2019. Stakeholder
12
13 781 Engagement to Inform National Weather Service Hydrologic Products and Services to
14
15 782 Meet User Needs NOAA National Weather Service Water Resources Services Branch
16
17 783 and Office of Water Prediction.
18
19
20 784 <https://www.weather.gov/media/water/StakeholderEngagementtoInformNWMProducts>
21
22 785 [Services2019.pdf](https://www.weather.gov/media/water/StakeholderEngagementtoInformNWMProducts/Services2019.pdf)
23
24
25 786 Pelissier, C., J. Frame, and G. Nearing, 2019. Combining Parametric Land Surface Models
26
27 787 with Machine Learning. arXiv preprint arXiv:2002.06141.
28
29
30
31 788 Read, J. S., Jia, X., Willard, J., Appling, A. P., Zwart, J. A., Oliver, S. K., et al. 2019.
32
33 789 Process-guided deep learning predictions of lake water temperature. *Water Resources*
34
35 790 *Research*, 55, 9173–9190. <https://doi.org/10.1029/2019WR024922>
36
37
38 791 Reichstein, M., G. Camps-valls, B. Stevens, M. Jung, J. Denzler, and N. Carvalhais, 2019.
39
40 792 Deep Learning and Process Understanding for Data-Driven Earth System Science.
41
42 793 *Nature* 566: 195–204. <https://doi.org/10.1038/s41586-019-0912-1>.
43
44
45
46 794 Salas, F. R., M. A. Somos-Valenzuela, A. Dugger, D. R. Maidment, D. J. Gochis, C. H.
47
48 795 David, W. Yu, D. Ding, E. P. Clark, and N. Noman, 2018. Towards Real-Time
49
50 796 Continental Scale Streamflow Simulation in Continuous and Discrete Space. *Journal of*
51
52 797 *the American Water Resources Association* 54, no. 1: 7–27.
53
54
55 798 <https://doi.org/10.1111/1752-1688.12586>.
56
57
58
59
60

- 1
2
3 799 Steiger, J., and M. Browne, 1984. The Comparison of Interdependent Correlations between
4
5 800 Optimal Linear Composites. *Psychometrika* 49, no. 1: 11–24.
6
7 801 <https://doi.org/10.1017/CBO9781107415324.004>.
8
9
10 802 Sundararajan, M., A. Taly, and Q. Yan, 2017. Axiomatic Attribution for Deep Networks.
11
12 803 34th International Conference on Machine Learning, ICML 2017 7: 5109–18.
13
14
15
16 804 Tartakovsky, A. M., C. O. Marrero, P. Perdikaris, G. D. Tartakovsky, and D. Barajas-
17
18 805 Solano, 2020. Physics-Informed Deep Neural Networks for Learning Parameters and
19
20 806 Constitutive Relationships in Subsurface Flow Problems. *Water Resources Research*
21
22 807 56, no. 5: 1–16. <https://doi.org/10.1029/2019WR026731>.
23
24
25
26 808 Xia, Y., K. Mitchell, M. Ek, J. Sheffield, B. Cosgrove, E. Wood, L. Luo, C. Alonge, H.
27
28 809 Wei, J. Meng, B. Livneh, D. Lettenmaier, V. Koren, Q. Duan, K. Mo, Y. Fan, and D.
29
30 810 Mocko, 2012. Continental-Scale Water and Energy Flux Analysis and Validation for
31
32 811 the North American Land Data Assimilation System Project Phase 2 (NLDAS-2): 1.
33
34 812 Intercomparison and Application of Model Products. *Journal of Geophysical Research*
35
36 813 *Atmospheres* 117, no. 3. <https://doi.org/10.1029/2011JD016048>.
37
38
39
40 814 Ye, A., Q. Duan, X. Yuan, E. F Wood, and J. Schaake, 2014. Hydrologic Post-Processing
41
42 815 of MOPEX Streamflow Simulations. *Journal of Hydrology* 508: 147–56.
43
44 816 <https://doi.org/10.1016/j.jhydrol.2013.10.055>.
45
46
47
48
49
50
51
52
53
54
55
56
57
58
59
60